Organic & Biomolecular Chemistry

Cite this: *Org. Biomol. Chem.*, 2011, **9**, 2885

www.rsc.org/obc

PAPER

The SAMP alkylation: A computational study†‡

Rainer Koch*

Received 6th December 2010, Accepted 1st February 2011
DOI: 10.1039/c0ob01125h

In a computational study of a stereoselective C–C bond formation, the SAMP alkylation, a previously proposed S_E2'-front mechanism is evaluated taking into account all current experimental evidence. Using semiempirical, density functional and perturbation theoretical methods, the structure of the key intermediate is revealed and the metalloretentive nature of the mechanism is explained. The experimental *ee* values of a range of reactions with different electrophiles and carbonyl sources can be correlated with calculated differences in activation energies. Furthermore, it can be concluded that the selectivity derives from the internal stabilization of the transition state **3_syn** (corresponding to an electrophilic attack from above the lithiohydrazone plane) by electrophile–lithium interactions. The fast computational approach can be used best as a screening method which excludes less promising candidates to guide this synthetic method.

Introduction

Among the most important organic reactions are those which form stereoselectively one or more new bonds.[1] Of particular interest are efficient and highly selective methods for C–C bond formation which introduce new stereogenic centers. The synthesis of an optically pure product in quantitative yields is still the holy grail in asymmetric synthesis, and there are only very few reactions which come close, *i.e.* use of only catalytic amounts of a chiral compound.

Procedures that allow the generation of new C–C bonds in the α position to a carbonyl group and simultaneously introduce new centers of chirality at the α- and/or β-positions are among the most important synthetic operations in organic chemistry. Typical problems of this carbonyl chemistry are solved nowadays with the introduction of metalated enolates,[2] azaenolates[3] or hydrazones[4] as reactive intermediates. In particular the latter has found widespread application because of its excellent yields and mild reaction conditions. One remarkable representative is the SAMP/RAMP hydrazone method:[5] Hydrazones derived from (*S*)-1-amino-2-methoxymethylpyrrolidine (SAMP) and ketones or aldehydes can be metalated and alkylated with broad generality, leading to α-alkylated carbonyl compounds in high enantiomeric purity.

Although much emphasis has been placed on the study of this and related newer approaches both experimentally[6] and theoretically,[7] a mechanism for this fascinating reaction has been postulated based only on the stereochemical outcome of the reaction. In order to shed some light on the mechanism of this synthetically very useful application and to additionally be able to predict the stereoselective outcome of previously unknown variations of this reaction, various quantum chemical methods have been employed in this work.

Computational details

Ab initio calculations were performed using the Gaussian 03 program package,[8] and the semiempirical calculations were run using the program MOPAC93/PC.[9] Geometries were optimized at PM3[10,11] and at B3LYP/6-31G(d)[12,13] levels of theory, and the nature of these stationary points confirmed as local minima or first-order transition states by calculation of vibrational frequencies at the corresponding level. Additional single point calculations at the MP2/6-31+G(d) level[14] based on B3LYP/6-31G(d) geometries were performed to obtain more reliable energies, while B3LYP/6-31G(d)//PM3 single points test the reliability of the semiempirical approach. A self-consistent reaction field (SCRF) approach using the default settings (COSMO[15] in MOPAC; PCM[16] in Gaussian 03) with the solvent explicitly set to water was used to model the influence of implicit solvation. Population analysis has been carried out using the natural bond order (NBO) version 5.G,[17] which is implemented in our local version of Gaussian 03.

Results and discussion

The utilization of (*S*)-1-amino-2-methoxymethylpyrrolidine (or SAMP) and its *R*-enantiomer RAMP as an auxiliary in asymmetric synthesis with carbon–carbon bond formation is now more than 30 years old. Enders first reported this variant of the hydrazone technique in 1976.[18] Mixing the chiral auxiliary with

Institut für Reine und Angewandte Chemie and Center of Interface Science, Carl von Ossietzky Universität Oldenburg, P.O. Box 2503, 26111, Oldenburg, Germany. E-mail: rainer.koch@uni-oldenburg.de; Fax: +49-441-798-193653; Tel: +49-441-798-3653

† Electronic supplementary information (ESI) available: Table of absolute energies of all calculated structures and the cartesian coordinates of all structures. See DOI: 10.1039/c0ob01125h

‡ Dedicated to Prof. Ernst Anders on the occasion of his 70th birthday

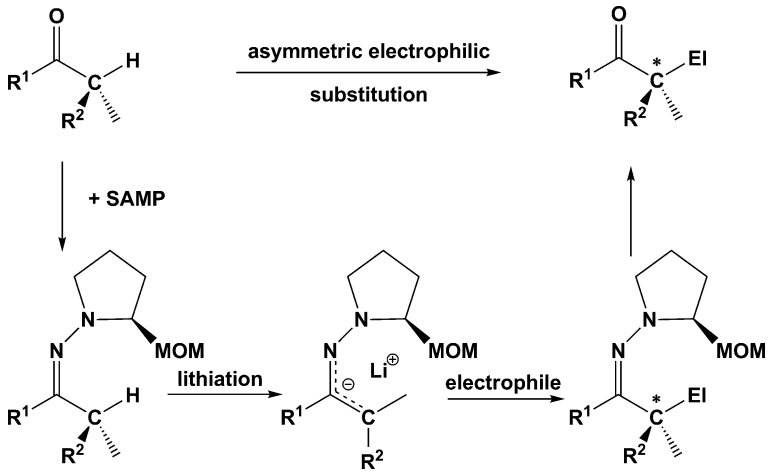

Scheme 1 Generalized mechanism of the SAMP reaction.

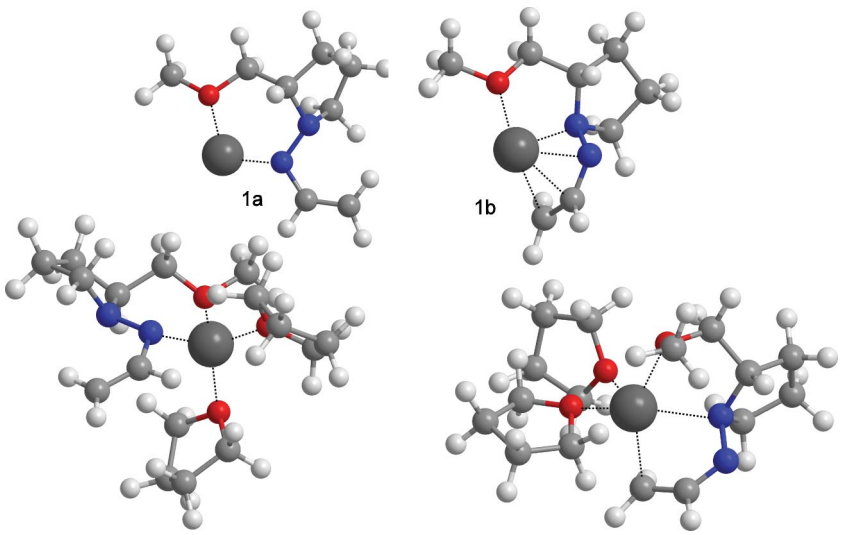

Fig. 1 Postulated model lithio azaenolates as key intermediates in the SAMP alkylation. The disolvated (THF) structures are shown in the lower half.

a carbonyl compound yields a chiral hydrazone. Deprotonation with a lithium base, typically LDA, leads to azaenolates which can be trapped by electrophiles to obtain diastereomerically enriched products. There have been several studies investigating the nature of the key intermediate, the lithiated azaenolate: it is known from freezing point depression and NMR experiments that it exists in a monomeric structure, probably complexed by two THF molecules.[19] Further data from X-ray analysis[20] and mechanistic studies[21] sheds little light on it and only indicates the coordination of the lithium cation to the oxygen atom of the methoxymethyl chain and an arrangement of the azaenolic part as shown in Scheme 1: an *E* orientation of the allylic C–C bond, *i.e.* N and R^2 on opposite sides, and a Z_{CN} orientation (C=R^2 and pyrrolidine on the same side).

It is essential to have a detailed knowledge of the structure of the intermediate metalated SAMP hydrazone in order to understand the mechanism. The first step was therefore to find a reliable geometry of a model key intermediate—formed from acetaldehyde and SAMP—within the experimental "constraints": many different arrangements which have the abovementioned MOM coordination of the lithium cation and the Z_{CN} orientation in common, have been trialed. The resulting two families of structures (several geometries for each type with very similar energies are found) possess a N–Li coordination as found in the X-ray structure, but with a varying number of additional contacts to the allylic carbon atoms and the second hydrazone nitrogen atom (Fig. 1). Unsurprisingly, structure **1b** with the most coordinations is predicted to be more stable in the gas phase, 62 kJ mol^{-1} lower in energy compared to **1a** at our best level of theory (MP2/6-311++G(d,p)//MP2/6-31G(d) level of theory).[22,23]

It is well-known that explicit solvation (or microsolvation) plays a crucial role in lithium chemistry[7d,f,24] and therefore needs to be taken into account. Based on literature and own experience, PM3 is generally considered to give reliable geometries, energies at this semiempirical level usually lead to barriers that are too high, so that B3LYP/6-31G(d)//PM3 or B3LYP/6-31G(d)//B3LYP/6-31G(d) energies should be preferred[7b,d,25] and are employed herein. A series of calculations on the model lithio azaenolate with one and two THF molecules has been performed. Several starting structures with THF attachment in different orientations were optimised and again lead to two sets of different geometries: one in which the lithium cation sits "above" the NNCC moiety and one

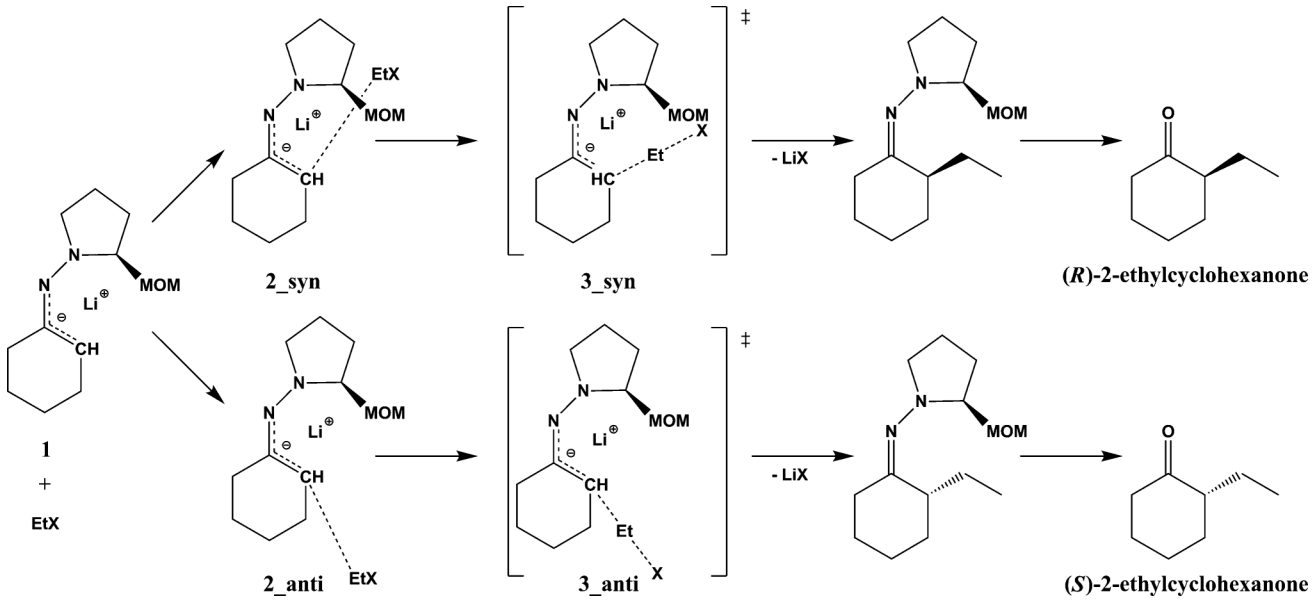

Scheme 2 SAMP alkylation of cyclohexanone with ethyl halide, see text for details.

where it is displaced to the "back" of this NNCC semicircle (Fig. 1 bottom, left and right). Attempts to locate additional structures always led to one of these two types. The energy difference between the two structures is reduced to less than 30 kJ mol^{-1} when adding one THF molecule. With the second solvent molecule the Li–O contacts become more important than those to the azaallylic part of the hydrazone, leading to almost equally stable structural motifs with three Li–O contacts (2 × THF and 1 × ether oxygen atom) within 8 kJ mol^{-1}. They differ only slightly in the distances and number of azaallylic contacts (Fig. 1, bottom). Both solvation steps are exothermic; hence this disolvated model complex will be used in the following, in line with cryoscopic data.[19] These findings are consistent within all applied methods. A note of caution should be added here: clearly, the complete energy surface cannot be fully explored. However, with the careful optimisation of possible intermediate structures herein, it is a justifiable assumption based on experimental evidence that the rate-determining step of the SAMP alkylation proceeds *via* this intermediate.

The stereochemistry of the resulting products of the SAMP alkylation indicates that the electrophiles predominantly attack the intermediate from the side where the lithium cation is coordinated. Together with the afore-mentioned experimental data, this has led to the postulation that the mechanism should be described as a metalloretentive S_E2'-front mechanism.[5a,19b,26]

To confirm this, the mechanism of the highly selective electrophilic substitution of cyclohexanone with ethyl halides under SAMP conditions (*ee* > 98%, Scheme 2)[5a,18a] has been calculated with different methods: starting from a lithio azaenolate, the alkyl halide (alkyl chloride instead of the experimentally utilized alkyl iodide is chosen in the calculations for computational reasons) can approach the azaallylic moiety from either above or below (Scheme 3), leading to two distinct pre-reaction complexes **2** and subsequently to two transition states **3** which yield two different diastereomeric intermediates and finally the two enantiomeric products. Nomenclature throughout this manuscript will be the following: structures are named **_syn** and **_anti** corresponding to

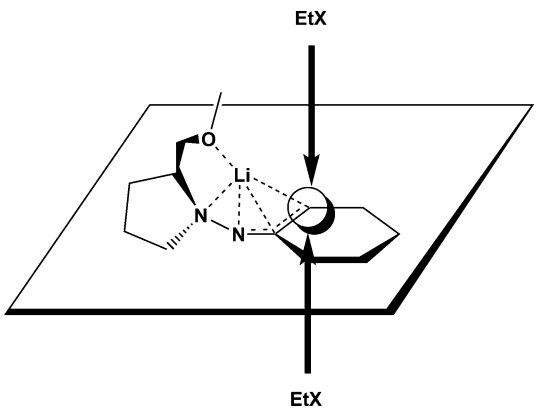

Scheme 3 Schematic presentation of the two possible electrophilic attack modes on a lithiated cyclohexylhydrazone.

the approach of the electrophile on the same side (*syn*, above the plane in Scheme 3) as the lithium cation or from the opposite side (*anti*, below the plane). Optimisation attempts starting from the two types of lithiated hydrazones (Fig. 1) resulted in the same transition state[27] so that there is a high degree of confidence that the transition states reported are in fact those which control the reaction.

The resulting transition states **3** are given in Fig. 2. One can clearly see the S_N2-type planarisation of the halide-bearing carbon atom in the electrophile and the coordination environment of the lithium cation. The energies for this prototype reaction are different levels of theory are summarized in Table 1.

There is the expected stabilization by a few kJ mol^{-1} of an adduct complex between the lithiated cyclohexanone-SAMP hydrazone and EtCl. Furthermore, the activation energy required for a top-side electrophile approach is consistently smaller compared to its counterpart **3_anti**. While the semiempirical method overestimates the barriers, it can be concluded that the PM3-predicted difference in activation energies for the two pathways is close to the "best"

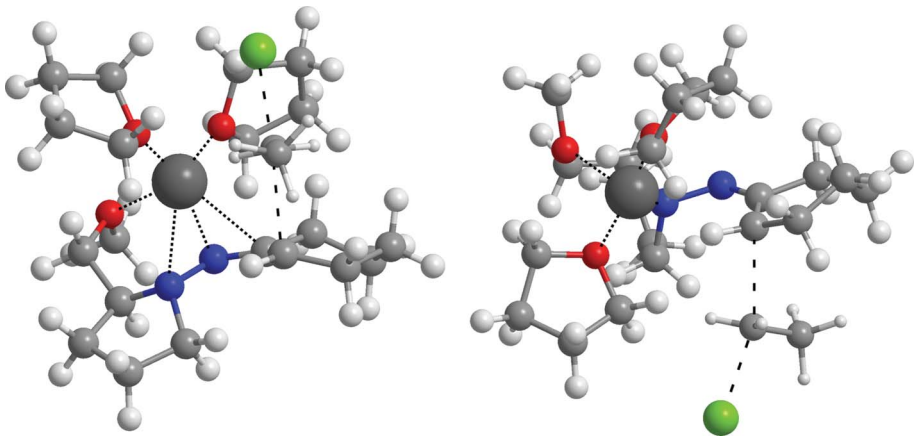

Fig. 2 Transition states **3_syn** (left) and **3_anti** (right) for the reaction of ethyl chloride with the lithiated cyclohexanone-SAMP hydrazone.

Table 1 Relative energies (kJ mol^{-1}) at different levels of theory for the prototype SAMP reaction and differences in activation energies (a positive $\Delta\Delta E^{\ddagger}$ value corresponds to a preference of **3_syn**, attack from above)

	PM3	B3LYP/6-31G(d)//PM3	B3LYP/6-31G(d)	MP2/6-31+G(d)//B3LYP/6-31G(d)
Reactants	0	0	0	0
2_syn	–18	6	–8	–32
2_anti	–22	6	16	–15
3_syn	108	54	69	58
3_anti	142	106	118	98
$\Delta\Delta E^{\ddagger}$	34	52	49	40

value (MP2/6-31+G(d)//B3LYP/6-31G(d).[28] The additional inclusion of an implicit solvent field does not change the overall picture; it leads only to slightly smaller differences in activation energies.[29] Note that the DFT single point calculations based on the PM3 geometries give low barriers in good agreement with the perturbation theory energies but at too high a difference ($\Delta\Delta E^{\ddagger}$).

Analysis of the geometries of both transition states calculated at the various levels of theory (Table 2) confirms the above-mentioned good agreement between PM3- and B3LYP/6-31G(d)-optimized geometries. In all cases, there are three strong lithium atom contacts to the ether O atoms (at around 2.0 Å). The lithium atom is usually attached to the azaallylic part with one or two Li–N interactions (<2.5 Å), in line with a tetrahedral coordination, while no close contacts are found to carbon atoms, as a result of the THF coordination. PM3 calculates Li–N distances which are predicted shorter than those optimized with the DFT method. This is not surprising as the length of a lithium contact is very sensitive (a few kJ mol^{-1} can prove decisive) and PM3—although optimized for lithium organic compounds—has some minor shortcomings handling benzyl lithium and slightly overestimates the strength of Li–N contacts.[11,30] The other bond lengths and distances calculated for the two transition states are in the expected range and compare well between all methods herein (PM3 gives somewhat longer Li distances, while the bond breaking/forming C–C distances are predicted shorter).

These data, together with the predicted energies in Table 1 and the superior feasibility of the semiempirical approach lead to the expectation that PM3, complemented by DFT single point calculations is suitable for activation barrier determination

Table 2 Selected bond lengths and distances (Å) of the two transition states **3_syn** and **3_anti** at different levels of theory

	3_syn		**3_anti**	
	B3LYP/6-31G(d)	PM3	B3LYP/6-31G(d)	PM3
Li–N_1[a]	2.816	2.407	2.122	2.311
Li–N_2	2.054	2.268	3.108	3.302
Li–C_1	2.831	3.123	3.311	3.551
Li–C_2	3.866	3.862	3.026	3.158
Li–O_{THF}	1.978/2.010	2.050/2.077	1.986/1998	2.032/2.041
Li–O_{MOM}	2.004	2.108	2.056	2.095
Li–C_A	3.811	3.663	4.331	4.048
Li–C_B	5.100	4.656	5.425	5.426
C_1–C_2	1.503	1.487	1.502	1.481
C_2–C_A	2.487	2.175	2.413	2.185
C_A–Cl	2.300	2.209	2.304	2.218
Li–Cl	4.507	4.368	5.774	5.046
Li–H_A	2.859	2.582	3.628	3.494

[a] For numbering see Scheme 2; C_A is the methylene and C_B the methyl carbon atom in ethyl chloride.

of other SAMP alkylations, at least for the relative energy differences.[31]

In the next step, we calculated the transition states for several other SAMP alkylations[5] with known enantiomeric excesses, covering a wide range of enantiomeric purities. In Table 3, reactions with different electrophiles, acyclic and cyclic carbonyl compounds, saturated and unsaturated cyclic ketones together with their *ee* values and the calculated difference in activation barriers are collected. The influence of both the zero-point energies and thermal corrections on the property of interest, the $\Delta\Delta E^{\ddagger}$ value, as well as the differences in entropic contributions, is negligible (0–2 kJ mol^{-1}), therefore free energies are not considered in the following.

The first important finding is that all reaction products are formed from a *syn* attack of the electrophile from above (as explained in Scheme 3), with the exception of the last entry in Table 3 where the stereochemical outcome depends on the reaction conditions. A few issues should be pointed out: There is significant influence of the solvent used, as can be seen for the reaction of 3-pentanone with EtCl: 60% *ee* in THF *vs.* 94% *ee* in Et_2O. Also, the electrophile can change the purity of the final

Table 3 Selected SAMP alkylations, *ee* values (%) and differences in activation energies (positive values correspond to a higher barrier for the anti attack from below, kJ mol^{-1})

Ketone	Electrophile	Product	Attack	*ee*	$\Delta\Delta E^{\ddagger}$ PM3	$\Delta\Delta E^{\ddagger}$ DFT[a]
Cyclohexanone	EtCl	(*R*)-2-ethylcyclohexanone	*syn*	98	34	52
Cyclohexanone	MeCl	(*R*)-2-methylcyclohexanone	*syn*	99	35	53
Cyclohexanone	AllylCl	(*S*)-2-allylcyclohexanone	*syn*	73	31	54
Cyclohexenone	MeCl	(*R*)-2-methylcyclohexenone	*syn*	61–75	26	45
3-pentanone	EtCl	(*S*)-4-methyl-3-hexanone	*syn*	60[b]	21	61
1-phenyl-2-propanone	MeCl	(*R*)-3-phenyl-2-butanone	*syn*	20	20	51
1,3-diphenyl-2-propanone	MeCl	1,3-diphenyl-2-butanone[c]	(*S*) *anti*	30	19	43
			(*R*) *syn*	11		

[a] B3LYP/6-31G(d)//PM3. [b] 94% in diethyl ether. [c] Products with different configuration are obtained, depending on reaction conditions.

product: dimethyl sulfate and methyl chloride yield *ee* values of the (*R*)-2-methylcyclohexanone formation between 67 and 99%. It is also worth mentioning that enantiomeric purities drop when a phenyl group is attached directly to the newly formed stereogenic center.

Keeping in mind that the experimental determination of chirality itself is error-prone and *ee* values depend on the reaction conditions (see above), a comparison between calculated and experimental differences in activation barriers for the two pathways seems difficult. The data in Table 3 however suggest that there is some kind of correlation between the calculated data and those derived from the enantiomeric purities: a large difference generally leads to a large enantiomeric excess, and on the other side a small gap is also reflected in the less selective outcome of the reaction. In Fig. 3, the experimental enantiomeric excess values are converted into an "experimental activation energy difference"[32] and compared to the calculated ones, demonstrating this correlation, at least for the PM3 data.[33] It should be pointed out that all calculated $\Delta\Delta E^{\ddagger}$ values are systematically too high. Changes in selectivity arising from different reaction conditions cannot be reproduced due to the nature of the computational model.

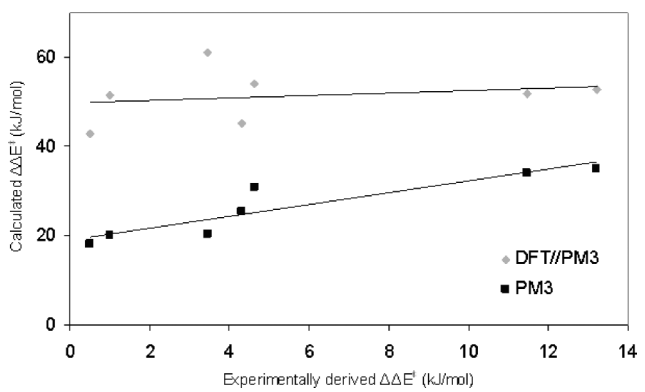

Fig. 3 Correlation between experimentally determined (derived from *ee* values) and calculated differences in activation energies.

It can be concluded that the correct sense of induction is observed in all cases, but the variations noted experimentally by changing the electrophile or conditions cannot be reproduced. It is also worth mentioning that the calculated barriers are in the range of 60–100 kJ mol^{-1} (see ESI† for details) and therefore have clearly the correct magnitude when comparing with the experimental conditions (–100° to 0 °C), supporting the validity of the proposed mechanism.

In all but one case the metalloretentive *syn* attack of the electrophile from above onto the allylic moiety is preferential. How can this observation be rationalized? The most striking difference from a visual inspection of the two types of transition states is the proximity of the lithium cation to the bond-breaking and bond-forming centers in **3_syn**, compared to **3_anti** (Fig. 2), and, additionally, there is always a larger number of contacts between the lithium atom and the azaallylic part (Table 2). Steric reasons can be ruled out as the reaction centers in both pathways are not shielded by a group in the vicinity. If hindrance would play any role at all, it should favor the attack from below as the position of the THF-solvated lithium cation gives rise to some crowding above the plane, which can be seen in Fig. 2. It can therefore be concluded that the aforementioned weak interactions between the lithium cation and the incoming electrophile and the stronger link to the azaallylic system lead to the observed stabilizing effect of the lithium cation on the transition state **3_syn**.[34] All these data suggest an S_E2-front- or S_Ei-type mechanism which are difficult to distinguish. The relatively large distance between reaction center (electrophile) and leaving group suggests that the former mechanism is more likely. One could also argue about an allylic double-bond shift, the short Li–N contacts in **3_syn** and the bond length changes in the azaallylic system support the occurrence of an S_E2' mechanism.

As pointed out above, there is a reduced (or even a reversed) selectivity when a phenyl group in the carbonyl compound is involved. Fig. 4 shows the reason for this behavior. In contrast

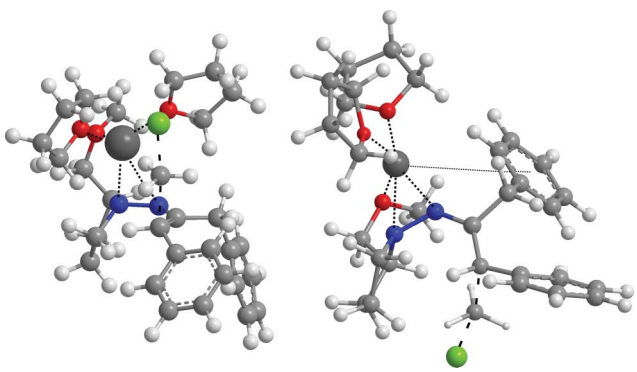

Fig. 4 Transition states (**3_syn** left, **3_anti** right) for the reaction with phenyl group-bearing carbonyl compounds illustrating the additional π–Li interactions.

to the normal situation where the electrophile approach from below does not experience any stabilization, a phenyl group can now interact with the lithium cation (π – 2 s) which leads to the observed shift in preference of the attacking mode.

Conclusions

The computational study of the SAMP alkylation leads to a mechanism which is in agreement with all current experimental evidence and supports the postulated S_E2'-front mechanism. Based on a solid theoretical foundation, it can reproduce the observed trend in stereoselectivities for a range of substrates and electrophiles, using the semiempirical method PM3 and B3LYP/6-31G(d)//PM3. The purpose of the employed approaches is clearly to provide a tool to quickly evaluate carbonyl compounds for their potential to undergo electrophilic substitution with high stereoselectivity and to exclude unpromising candidates from synthesis. Furthermore, it can be concluded that the selectivity derives from the internal stabilization of the transition state **3_syn** (corresponding to the electrophilic attack from above the lithiohydrazone plane) by electrophile–lithium interactions; steric effects do not play a role.

Acknowledgements

In particular, I gratefully thank Prof. E. Anders for his invaluable support and ongoing fruitful discussions, in particular during the early stages of my career. This work was supported by computer time at the Centre for Scientific Computing at the University of Oldenburg. Financial assistance from the DFG is gratefully acknowledged.

References

1 (*a*) G. Helmchen, R. W. Hoffmann, J. Mulzer and E. Schaumann, (ed.) *Houben-Weyl Stereoselective Synthesis*, Thieme, Stuttgart, 4th edn, 1996, vol. E21; (*b*) E. N. Jacobsen, A. Pfaltz and H. Yamamoto, (ed.) *Comprehensive Asymmetric Catalysis*, Springer, New York, 1999; (*c*) D. Enders and K.-E. Jaeger, (ed.) *Asymmetric Synthesis with Chemical and Biological Methods*, Wiley-VCH, Weinheim, 2007.

2 D. A. Evans, in *Asymmetric Synthesis*; ed. J. D. Morrison, Academic Press, Orlando, 1983–1984, vol. 3 pp. 1–110 and references cited therein.

3 (*a*) G. Wittig and A. Hesse, *Org. Synth.*, 1970, **50**, 66–72; (*b*) G. Stork and S. R. Dowd, *Org. Synth.*, 1974, **54**, 46–49.

4 (*a*) F. E. Henoch, K. G. Hampton and C. R. Hauser, *J. Am. Chem. Soc.*, 1967, **89**, 463; (*b*) G. Stork and J. Benaim, *J. Am. Chem. Soc.*, 1971, **97**, 5938–5939; (*c*) G. Stork and J. Benaim, *Org. Synth.*, 1977, **57**, 69–72; (*d*) E. J. Corey and D. Enders, *Chem. Ber.*, 1978, **111**, 1337–13611362–1383; (*e*) R. Lazny and A. Nodzewska, *Chem. Rev.*, 2010, **110**, 1386–1434.

5 For reviews on the SAMP method see: (*a*) D. Enders, in *Asymmetric Synthesis*, ed. J. D. Morrison, Academic Press, Orlando, 1983–1984, vol. 3 pp. 275–339; (*b*) A. Job, C. F. Janeck, W. Bettray, R. Peters and D. Enders, *Tetrahedron*, 2002, **58**, 2253–2329and references therein; (*c*) D. Enders and W. Bettray, in *Asymmetric Synthesis – The Essentials*, ed. S. Bräse and M. Christmann, Wiley-VCH, Weinheim, 2007, pp. 23–29.

6 (*a*) S. E. Denmark, T. Weber and D. W. Piotrowski, *J. Am. Chem. Soc.*, 1987, **109**, 2224–2225; (*b*) D. Enders, H. Wahl and W. Bettray, *Angew. Chem.*, 1995, **107**, 527–529, (*Angew. Chem., Int. Ed. Engl.*, 1995, **34**, 455); (*c*) D. Enders, E. Díez, R. Fernández, E. Martín-Zamorra, J. M. Muñoz, R. R. Pappalardo and J. M. Lassaletta, *J. Org. Chem.*, 1999, **64**, 6329–6336; (*d*) D. Enders, S. F. Müller, G. Raabe and J. Runsink, *Eur. J. Org. Chem.*, 2000, 879–892; (*e*) B. List, R. A. Lerner and C. F. Barbas III, *J. Am. Chem. Soc.*, 2000, **122**, 2395–2396; (*f*) N. Halland, M. Alstrup Lie, A. Kjærsgaard, M. Marigo, B. Schiøtt and K. A. Jørgensen, *Chem.–Eur. J.*, 2005, **11**, 7083–7090; (*g*) D. Seebach, A. K. Beck, D. M. Badine, M. Limbach, A. Eschenmoser, A. M. Treasurywala, R. Hobi, W. Prikoszovich and B. Linder, *Helv. Chim. Acta*, 2007, **90**, 425–471; (*h*) P. Dinér, A. Kjærsgaard, M. Alstrup Lie and K. A. Jørgensen, *Chem.–Eur. J.*, 2008, **14**, 122–127; (*i*) N. Duguet, S. M. Petit, P. Marchand, A. Harrison-Marchand and J. Maddaluno, *J. Org. Chem.*, 2008, **73**, 5397–5409; (*j*) S. E. Denmark and J. J. Ares, *J. Org. Chem.*, 2008, **73**, 9647–9656.

7 (*a*) R. Glaser and A. Streitwieser, *J. Am. Chem. Soc.*, 1987, **109**, 1258–1260; (*b*) L. M. Pratt and I. M. Khan, *J. Comput. Chem.*, 1995, **16**, 1067–1080; (*c*) M. Feigel, G. Martinek and W. H. B. Sauer, *Chem.–Eur. J.*, 1996, **2**, 9–18; (*d*) A. Abbotto, A. Streitwieser and P. R. v. Schleyer, *J. Am. Chem. Soc.*, 1997, **119**, 11255–11268; (*e*) V. Ojea, M. Ruiz, G. Shapiro and E. Pombo-Villar, *J. Org. Chem.*, 2000, **65**, 1984–1995; (*f*) L. M. Pratt and A. Streitwieser, *J. Org. Chem.*, 2003, **68**, 2830–2838; (*g*) K. Ando, *J. Am. Chem. Soc.*, 2005, **127**, 3964–3972; (*h*) B. De Sterck, V. Van Speybroeck, S. Mangelinckx, G. Verniest, N. De Kimpe and M. Waroquier, *J. Phys. Chem. A*, 2009, **113**, 6375–6380.

8 M. J. Frisch, G. W. Trucks, H. B. Schlegel, G. E. Scuseria, M. A. Robb, J. R. Cheeseman, J. J. A. Montgomery, T. Vreven, K. N. Kudin, J. C. Burant, J. M. Millam, S. S. Iyengar, J. Tomasi, V. Barone, B. Mennucci, M. Cossi, G. Scalmani, N. Rega, G. A. Petersson, H. Nakatsuji, M. Hada, M. Ehara, K. Toyota, R. Fukuda, J. Hasegawa, M. Ishida, T. Nakajima, Y. Honda, O. Kitao, H. Nakai, M. Klene, X. Li, J. E. Knox, H. P. Hratchian, J. B. Cross, V. Bakken, C. Adamo, J. Jaramillo, R. Gomperts, R. E. Stratmann, O. Yazyev, A. J. Austin, R. Cammi, C. Pomelli, J. W. Ochterski, P. Y. Ayala, K. Morokuma, G. A. Voth, P. Salvador, J. J. Dannenberg, V. G. Zakrzewski, S. Dapprich, A. D. Daniels, M. C. Strain, O. Farkas, D. K. Malick, A. D. Rabuck, K. Raghavachari, J. B. Foresman, J. V. Ortiz, Q. Cui, A. G. Baboul, S. Clifford, J. Cioslowski, B. B. Stefanov, G. Liu, A. Liashenko, P. Piskorz, I. Komaromi, R. L. Martin, D. J. Fox, T. Keith, M. A. Al-Laham, C. Y. Peng, A. Nanayakkara, M. Challacombe, P. M. W. Gill, B. Johnson, W. Chen, M. W. Wong, C. Gonzalez and J. A. Pople, Gaussian, Inc., Pittsburgh PA, 2004.

9 J. J. P. Stewart, MOPAC 93; # 455, QCPE Bulletin, 1993. PC version: R. Koch, unpublished.

10 (*a*) J. J. P. Stewart, *J. Comput. Chem.*, 1989, **10**, 209–220; (*b*) J. J. P. Stewart, *J. Comput. Chem.*, 1989, **10**, 221–264.

11 Li parameters: E. Anders, R. Koch and P. Freunscht, *J. Comput. Chem.*, 1993, **14**, 1301–1312.

12 (*a*) A. D. Becke, *Phys. Rev. A: At., Mol., Opt. Phys.*, 1988, **38**, 3098–3100; (*b*) C. Lee, W. Yang and R. G. Parr, *Phys. Rev. B*, 1988, **37**, 785–789; (*c*) A. D. Becke, *J. Chem. Phys.*, 1993, **98**, 5648–5652.

13 (*a*) P. C. Hariharan and J. A. Pople, *Theor. Chim. Acta*, 1973, **28**, 213–222; (*b*) M. M. Francl, W. L. Pietro, W. L. Hehre, J. S. Binkley, M. S. Gordon, D. J. DeFrees and J. A. Pople, *J. Chem. Phys.*, 1982, **77**, 3654–3665.

14 (*a*) C. Møller and M. S. Plesset, *Phys. Rev.*, 1934, **46**, 618–622; (*b*) J. A. Pople, J. S. Binkley and R. Seeger, *Int. J. Quantum Chem.*, 1976, **10 S10**, 1–19 and references therein; (*c*) M. Head-Gordon, J. A. Pople and M. J. Frisch, *Chem. Phys. Lett.*, 1988, **153**, 503–506.

15 A. Klamt and G. Schüürmann, *J. Chem. Soc., Perkin Trans. 2*, 1993, 799–805.

16 (*a*) S. Miertus, E. Scrocco and J. Tomasi, *Chem. Phys.*, 1981, **55**, 117–129; (*b*) S. Miertus and J. Tomasi, *Chem. Phys.*, 1982, **65**, 239–245; (*c*) M. Cossi, V. Barone, R. Cammi and J. Tomasi, *Chem. Phys. Lett.*, 1996, **255**, 327–335; (*d*) M. T. Cancès, B. Mennucci and J. Tomasi, *J. Chem. Phys.*, 1997, **107**, 3032–3041; (*e*) M. Cossi, V. Barone, B. Mennucci and J. Tomasi, *Chem. Phys. Lett.*, 1998, **286**, 253–260.

17 NBO 5.G. E. D. Glendening, J. K. Badenhoop, A. E. Reed, J. E. Carpenter, J. A. Bohmann, C. M. Morales and F. Weinhold (Theoretical Chemistry Institute, University of Wisconsin, Madison, WI, 2004); http://www.chem.wisc.edu/~nbo5.

18 (*a*) D. Enders and H. Eichenauer, *Angew. Chem.*, 1976, **88**, 579–580, (*Angew. Chem. Int. Ed.*, 1976, **15**, 549–551); (*b*) D. Enders and H. Eichenauer, *Tetrahedron Lett.*, 1977, **18**, 191–194.

19 (*a*) W. Bauer and D. Seebach, *Helv. Chim. Acta*, 1984, **67**, 1972–1988; (*b*) D. Enders, *Chem. Scripta*, 1985, **25**, 139–147.

20 D. Enders, G. Bachstädter, K. A. M. Kremer, M. Marsch, K. Harms and G. Boche, *Angew. Chem.*, 1988, **100**, 1580–1581, (*Angew. Chem., Int. Ed. Engl.*, 1988, **27**, 1522).

21 (*a*) D. Enders and H. Eichenauer, *Chem. Ber.*, 1979, **112**, 2933–2960; (*b*) D. Enders, H. Eichenauer, U. Baus, H. Schubert and K. A. M. Kremer, *Tetrahedron*, 1984, **40**, 1345–1359.

22 In a combined X-ray and MNDO study, this structural motif has also been observed in a related aminoallyllithium compound: H. Ahlbrecht, G. Boche, K. Harms, M. Marsch and H. Sommer, *Chem. Ber.*, 1990, **123**, 1853–1858.
23 B3LYP/6-31G(d) calculations give an identical result: **1a** lies 62 kJ mol^{-1} above **1b**.
24 (*a*) Y. Balamraju, C. D. Sharp, W. Gammill, N. Manuel and L. M. Pratt, *Tetrahedron*, 1998, **54**, 7357–7366; (*b*) L. M. Pratt and S. Robbins, *THEOCHEM*, 1999, **466**, 95–101; (*c*) M. Piffl, J. Weston, W. Gunther and E. Anders, *J. Org. Chem.*, 2000, **65**, 5942–5950; (*d*) S. Mogali, K. Darville and L. M. Pratt, *J. Org. Chem.*, 2001, **66**, 2368–2373; (*e*) J. M. Saá, *Helv. Chim. Acta*, 2002, **85**, 814–840; (*f*) L. M. Pratt, D. G. Truhlar, C. J. Cramer, S. R. Kass, J. D. Thompson and J. D. Xidos, *J. Org. Chem.*, 2007, **72**, 2962–2966.
25 (*a*) R. Koch and E. Anders, *J. Org. Chem.*, 1995, **60**, 5861–5866; (*b*) R. Koch, B. Wiedel and E. Anders, *J. Org. Chem.*, 1996, **61**, 2523–2529; (*c*) P. I. Arvidsson, G. Hilmersson and P. Ahlberg, *J. Am. Chem. Soc.*, 1999, **121**, 1883–1887; (*d*) C. J. Hayes, N. S. Simpkins, D. T. Kirk, L. Mitchell, J. Baudoux, A. J. Blake and C. Wilson, *J. Am. Chem. Soc.*, 2009, **131**, 8196–8210.
26 To due the poor quality of the lithium parameters, early unpublished MNDO results by Andrade and Schleyer are not reliable enough to provide additional insight (see for example ref. 5, p. 327).
27 In the *syn* transition states (electrophile and Li^+ on the same side) the lithium cation is located over the central CN bond of the NNCC moiety, closer to its back, similarly to **1a** in Fig. 1, making way for the incoming electrophile. When the lithium cation and the electrophile are on opposite sides, Li+ is chelated by the NNCC as in **1b**. This is consistent for all calculated reactions in Table 3.
28 The "best" approach benefits from a possible cancellation of errors as the employed DFT method under- and MP2 overestimates dispersion effects.
29 This is consistent also for all calculated reactions in Table 3 and hence does not explain the observed directional change of the incoming electrophile.
30 R. Koch, B. Wiedel and E. Anders, *J. Org. Chem.*, 1996, **61**, 2523–2529.
31 Although the B3LYP/6-31G(d)//PM3 level of theory has been successfully applied to various lithium chemistry problems (see for example ref.7b,d and 25), large errors on other systems cannot be ruled out.
32 The enantiomeric excess *ee* is defined as $ee = (1-r_x/r_y)/(1+r_x/r_y)$ with the relative product rate $r_x/r_y = \exp(-\Delta\Delta E_a/RT)$.
33 B3LYP/6-31G(d)//PM3 predicts a too large barrier difference for the ethylation of 3-pentanone, the remainder of the data follow the described trend.
34 This is supported by an NBO analysis which shows weak donating interactions from the electrophile to the almost empty Li 2 s orbital only in the transition state **3_syn**.